Hydroxo-Bridged Dicopper(II,III) and -(III,III) Complexes: Models for Putative Intermediates in Oxidation Catalysis

Mohammad Reza Halvagar,[†] Pavlo V. Solntsev,[†] Hyeongtaek Lim,[‡] Britt Hedman,[§] Keith O. Hodgson,[‡,§] Edward I. Solomon,[‡,§] Christopher J. Cramer,*,[†] and William B. Tolman*,[†]

[†]Department of Chemistry, Center for Metals in Biocatalysis, Chemical Theory Center, and Minnesota Supercomputing Institute, University of Minnesota, 207 Pleasant Street SE, Minneapolis, Minnesota 55455, United States

[‡]Department of Chemistry, Stanford University, Stanford, California 94305, United States

[§]Stanford Synchrotron Radiation Lightsource, SLAC National Accelerator Laboratory, Stanford University, Menlo Park, California 94025, United States

S *Supporting Information*

ABSTRACT: A macrocyclic ligand (L^{4-}) comprising two pyridine(dicarboxamide) donors was used to target reactive copper species relevant to proposed intermediates in catalytic hydrocarbon oxidations by particulate methane monooxygenase and heterogeneous zeolite systems. Treatment of LH_4 with base and $Cu(OAc)_2 \cdot H_2O$ yielded $(Me_4N)_2[L_2Cu_4(\mu_4\text{-}O)]$ (**1**) or $(Me_4N)[LCu_2(\mu\text{-}OH)]$ (**2**), depending on conditions. Complex **2** was found to undergo two reversible 1-electron oxidations via cyclic voltammetry and low-temperature chemical reactions. On the basis of spectroscopy and theory, the oxidation products were identified as novel hydroxo-bridged mixed-valent Cu(II)Cu(III) and symmetric Cu(III)$_2$ species, respectively, that provide the first precedence for such moieties as oxidation catalysis intermediates.

Figure 1. Dicopper–oxygen cores proposed for pMMO (**A**–**C**) and Cu-zeolites (**D**), and the tetra-anionic ligand used in this work.

The selective functionalization of methane is well-recognized to be a "grand challenge" in catalysis science.[1,2] Among catalysts capable of converting methane to methanol, two of the most intriguing are particulate methane monooxygenase (pMMO)[3] and Cu-zeolites,[4] both of which are postulated to use copper–oxygen intermediates to attack the strong C–H bonds of CH_4. Significant evidence suggests that the active site of pMMO contains two proximal Cu ions,[5] although alternatives have been suggested.[6] Proposals for the nature of the oxidant in pMMO include **A**–**C** (Figure 1),[7,8] of which only **A** has been most thoroughly characterized in synthetic complexes;[9] examples of the mono-oxo dicopper-(II,II) core **D** have been prepared[10] and identified for Cu-ZSM5.[11] The preparation of complexes with cores like **A**–**D** represents a significant goal in efforts to test the feasibility and understand the fundamental chemistry of proposed intermediates in catalytic methane oxidations.

In previous work, we found that the strongly electron-donating pyridine(dicarboxamide) unit is well-suited for the isolation of reactive copper compounds, including a nucleophilic monocopper–superoxide complex,[12] monocopper(III)–hydroxide complexes that rapidly attack weak C–H bonds,[13,14] and a copper–hydroxide complex of a macrocyclic ligand that oxidizes tetrahydrofuran.[15] On the basis of these results, we
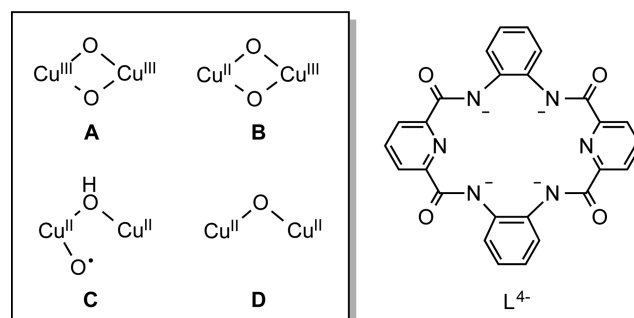
reasoned that dicopper–oxygen intermediates would be stabilized by ligand L^{4-} (Figure 1), which contains *two* such pyridine(dicarboxamide) donors within a macrocyclic frame. Herein, we report the synthesis and structural characterization of hydroxo-bridged dicopper(II,II) and (μ_4-O)tetracopper complexes supported by L^{4-}, and the stepwise 1-electron oxidations of the hydroxo-bridged complex to yield novel and reactive mixed-valent Cu(II)Cu(III) and Cu(III)Cu(III) compounds. These new motifs provide precedence for possible intermediates in catalytic hydrocarbon oxidations performed by dicopper sites.

In initial attempts to access the desired (μ-hydroxo)-dicopper(II,II) complex, $LH_4 \cdot DMF$ (prepared via a modification of a published procedure)[16] was treated with an excess of Me_4NOH (9 equiv) in MeOH, the deprotonated ligand was isolated, and it was then added to $Cu(OAc)_2 \cdot H_2O$ in water/pyridine (1:2 v/v). After workup and slow evaporation of a CH_3CN solution, green crystals were isolated (38%) and identified as $(Me_4N)_2[L_2Cu_4(\mu_4\text{-}O)]$ (**1**) on the basis of X-ray crystallography (Figure 2), negative-ion ESI-MS ($[M]^{2-}$ m/z 607.9), and CHN analysis. The di-anionic complex features a precedented[17] $[Cu_4(\mu_4\text{-}O)]^{6+}$ core bound by two L^{4-} ligands via their pyridine(dicarboxamide) donors.

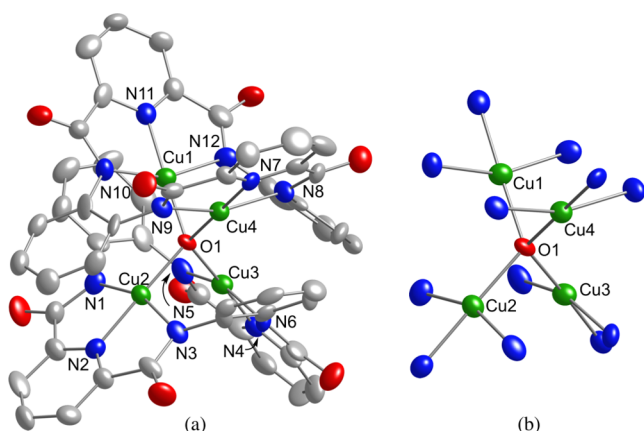By performing the reaction with less Me_4NOH (5 equiv) and slightly modifying the workup procedure, the dicopper complex

Figure 2. Representations of the di-anionic portion of the X-ray crystal structure of $(Me_4N)_2[L_2Cu_4(\mu_4\text{-}O)]$ (**1**), showing (a) the entire dianion and (b) the $[Cu_4(\mu_4\text{-}O)]^{6+}$ core and the supporting N-donor atoms. All non-hydrogen atoms are shown as 50% thermal ellipsoids, and all hydrogen atoms are omitted for clarity. Selected bond distances (Å) and angles (deg): Cu1–N11, 1.884(15); Cu1–O1, 1.920(10); Cu1–N12, 1.999(14); Cu1–N10, 2.015(14); Cu2–O1, 1.907(10); Cu2–N2, 1.918(14); Cu2–N3, 2.012(14); Cu2–N1, 2.039(14); Cu3–N6, 1.869(14); Cu3–O1, 1.915(11); Cu3–N4, 1.994(13); Cu3–N5, 2.016(14); Cu4–N8, 1.881(14); Cu4–O1, 1.925(10); Cu4–N9, 2.003(14); Cu4–N7, 2.030(14); Cu1–Cu4, 2.672(3); Cu2–Cu3, 2.669(3); Cu1–Cu2, 3.336(10); Cu1–Cu3, 3.330(10); Cu2–Cu4, 3.328(10); Cu2–O1–Cu3, 88.6(4); Cu2–O1–Cu1, 121.3(5); Cu3–O1–Cu1, 120.5(5); Cu2–O1–Cu4, 120.6(5); Cu3–O1–Cu4, 121.6(5); Cu1–O1–Cu4, 88.0(4).

$(Me_4N)[LCu_2(\mu\text{-}OH)]$ (**2**) was isolated. While **2** is stable as a solid, solutions of it in DMF decay gradually to **1** upon standing (1 d). The formulation of **2** was confirmed by X-ray crystallography (Figure 3), ESI-MS ($[M + Me_4N]^+$ m/z 765.0), and CHN analysis. Notable structural features include folding of the supporting ligand to generate an exposed (μ-hydroxo)dicopper(II,II) unit with a short Cu–Cu distance of 2.6596(15) Å and a Cu–OH–Cu angle of 89.0(2)°. Solutions of the complex in DMF are EPR silent (X-band, 30 K), consistent with antiferromagnetic coupling of the Cu(II) ions
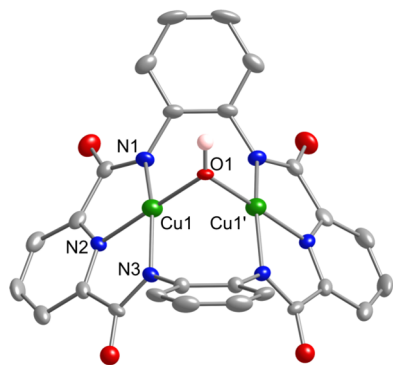

Figure 3. Representation of the anionic portion of the X-ray crystal structure of $(Me_4N)[LCu_2(\mu\text{-}OH)]$ (**2**), with all non-hydrogen atoms shown as 50% thermal ellipsoids and all hydrogen atoms except the hydroxide hydrogen omitted for clarity. Selected bond distances (Å) and angles (deg): Cu1–O1, 1.898(3); Cu1–N2, 1.909(4); Cu1–N1, 2.003(4); Cu1–N3, 2.006(4); Cu1–Cu1′, 2.6596(15); O1–Cu1–N2, 178.22(19); O1–Cu1–N1, 100.59(19); N2–Cu1–N1, 81.16(18); O1–Cu1–N3, 97.45(19); N2–Cu1–N3, 80.88(18); N1–Cu1–N3, 159.72(19); Cu1–O1–Cu1, 89.0(2).

that was confirmed by SQUID data for a powder sample (10–325 K, $2J = -11.5$ cm^{-1}, Figure S4). Optimization of **2** at the PBE0[18] level of density functional theory (DFT), including DMF solvation effects with the IEF-PCM solvation model[19] (see Supporting Information for full theoretical details), gives good structural agreement, e.g., Cu1–Cu1′, 2.657 Å; Cu1–O1, 1.940 Å, Cu1–O1–Cu1′, 86.5°, and it predicts a singlet ground state, with a singlet–triplet splitting of −61 cm^{-1}.

Cyclic voltammetry experiments performed on solutions of **2** (1 mM) in wet DMF (∼2% H$_2$O, 50 mM Bu$_4$NPF$_6$) revealed two reversible redox waves with $E_{1/2} = 0.18$ and 0.47 V vs Fc/Fc$^+$ (300 mV/s; $\Delta E_{pc,pa} = 72$ and 81 mV, respectively; $i_{pa}/i_{pc} \approx 1$; Figure 4a). These two waves may be ascribed to 1-electron

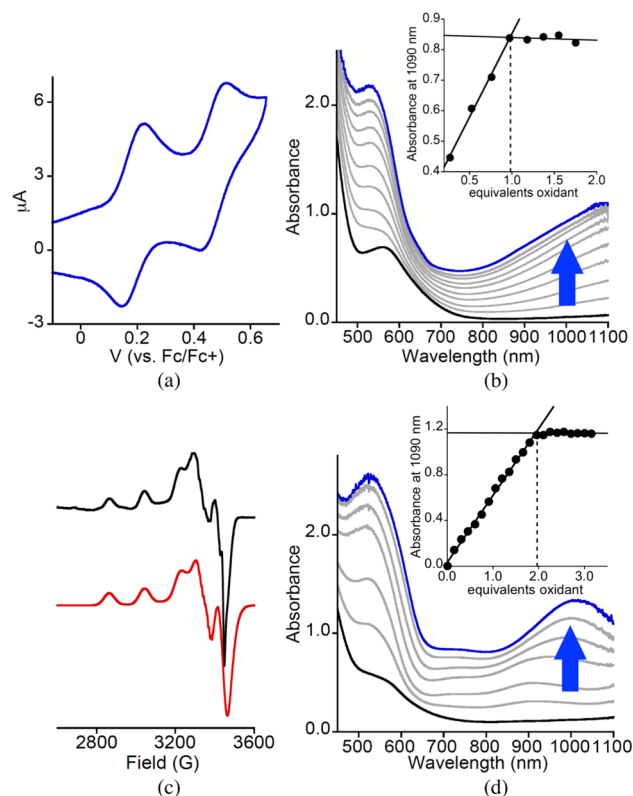**Figure 4.** (a) Cyclic voltammogram of **2** (see text for conditions). (b) UV–vis spectral changes as (AcFc)(SbF$_6$) is added to solution of **2** in DMF (1 mM) at −50 °C (black, **2**; blue, final species; gray, intermediate spectra), with titration data shown as the inset. (c) Experimental (black) and simulated (red) EPR spectra of product of reaction of **2** with (AcFc)(SbF$_6$) (9.64 GHz, 20 K; parameters $g_∥ = 2.210$, $g_⊥ = 2.054$, $A_∥(Cu) = 185 \times 10^{-4}$ cm^{-1}, $A_⊥(^{14}N) = 10 \times 10^{-4}$ cm^{-1}). (d) UV–vis spectral changes as CAN is added to a solution of **2** in DMF (0.5 mM) at −50 °C (black, **2**; blue, final species; gray, intermediate spectra), with titration data shown as the inset.

oxidations of **2** to formally Cu(II)Cu(III) and Cu(III)Cu(III) species. To further characterize these species, chemical oxidations of **2** were performed at −50 °C and monitored by UV–vis and EPR spectroscopy. Addition of acetylferrocenium hexafluoroantimonate, (AcFc)(SbF$_6$), to a DMF solution of **2** resulted in a shift and intensity increase of the band at $\lambda_{max} = 570$ nm to a new feature at 528 nm ($\varepsilon \approx 2150$ M^{-1} cm^{-1}), as well as the growth of a broad feature extending into the near-IR (Figure 4b). Titration experiments indicated that these new features reached maximum intensity upon addition of 1 equiv of (AcFc)(SbF$_6$), consistent with formation of a 1-electron-

oxidized intermediate. The spectral features decayed upon standing via a first-order process with $k = 3.1 \times 10^{-3}$ s^{-1} at -20 °C (Figure S6). This decay rate increases when dihydroanthracene is present, and anthracene was identified as a product by UV−vis and GC−MS (Figure S7). EPR spectra of the oxidized species featured a distorted axial signal with hyperfine splitting indicative of a single Cu(II) center (Figure 4c), consistent with a localized mixed-valent Cu(II)Cu(III) formulation **3** (Scheme 1).

Scheme 1. Proposed Products of Oxidations of 2
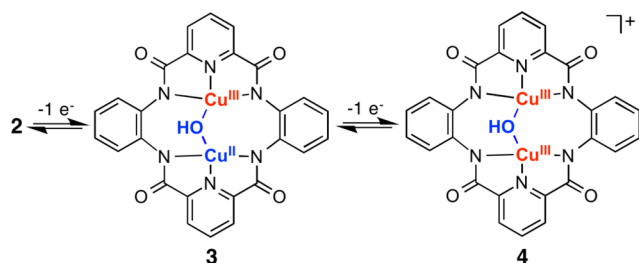
Treatment of a DMF solution of **2** with $(NH_4)_2Ce(NO_3)_6$ (ceric ammonium nitrate, CAN) at -50 °C yielded the UV−vis spectral changes shown in Figure 4d. The new feature at 525 nm is approximately twice as intense as that for the 1-electron-oxidized product of the reaction with $(AcFc)(SbF_6)$, and a unique feature at ~1000 nm is observed. These spectral features reach maximum intensity upon addition of 2 equiv of CAN, consistent with a 2-electron oxidation. The product solution is EPR silent and decays via a first-order process with a rate constant of 2.3×10^{-3} s^{-1} at -20 °C that increases when DHA is present (Figure S7). Finally, Cu K-edge XAS data for the oxidized species showed upward shifts in energy of the pre-edge and rising edge features by ~0.7 and ~1 eV, respectively, relative to **2** and the product of decomposition of the oxidized solution (Figure S8). These results are consistent with oxidation of the copper ions in the oxidized product. Taken together, the data are consistent with formation of a formally Cu(III)Cu(III) species **4** (Scheme 1).

To gain further insight into the structures of **3** and **4**, DFT calculations aimed at evaluating the geometries, ground states, redox potentials, and spectroscopic features were performed for these species assuming a hydroxo bridge. At the IEF-PCM/PBE0 level, the electronic ground states of **3** and **4** are predicted to be doublet and singlet, respectively, with corresponding quartet and triplet states predicted to be 1370 and 4420 cm^{-1} higher in energy. In **3**, the geometry distorts so that the two Cu atoms are not symmetrically coordinated, albeit with small differences between their geometries. Thus, the two Cu−O bond lengths are 1.930 and 1.910 Å, and the Cu−N bond lengths are ~0.01 Å shorter to the Cu atom having the shorter Cu−O bond length. The PBE0 singly occupied molecular orbital is primarily a $d_{x^2-y^2}$ on the copper atom having longer Cu−N/O bond lengths; the corresponding orbital on the other Cu atom is virtual, consistent with shorter Cu−N/O bond lengths, a formal Cu(III) assignment for this atom, and a localized mixed-valent formulation for **3** that is consistent with the EPR spectroscopic data. The Cu−Cu distance is 2.661 Å, and the Cu−O−Cu bond angle is 87.8°. In **4**, the calculations predict that symmetry is fully restored, with Cu−O bond distances of 1.864 Å, a Cu−Cu distance of 2.760 Å, and a Cu−O−Cu bond angle of 95.5°.

Evidence supporting a hydroxo rather than an oxo bridging group in the oxidized complexes comes from modeling the electrochemistry and UV−vis spectral data. DFT calculations at the SMD[20]/M11-L[21] level (which level has previously been shown[22] to be useful for the prediction of Pourbaix diagrams of coordination compounds in aqueous solution) predict potentials of 0.02 and 0.29 V vs Fc/Fc$^+$ for sequential 1-electron oxidations of **2** that are *not* accompanied by deprotonation (the pK_a of **4** is predicted to be about 8 on an aqueous scale). While the agreement between theory and experiment is only fair for the absolute redox potentials, the difference between them is quite well reproduced (expt, 290 mV; theory, 270 mV). These computations suggest that the bridge in **3** remains a hydroxo group, but they are inconclusive with respect to **4**, given the near-neutral pK_a that is predicted.

Considering the UV−vis spectra, time-dependent (TD) DFT calculations at the SMD/PBE0 level, including solvatochromic effects computed using the vertical electrostatic model,[23] provide good agreement with experiment for the middle-wavelength absorptions for **2** and **3** (Figure S9); peaks with moderate oscillator strength from 480 to 570 nm are predicted to be replaced by peaks in **3** ranging from 450 to 550, consistent with the blue shift observed with oxidation experimentally. Significant absorptions for **3** are also predicted at 910, 1083, and 1530 nm. In the case of **4**, the agreement between TD DFT and experiment is again quite good, with a long-wavelength absorption predicted at about 833 nm with strong LMCT character (note that the difference in energy for wavelengths of 833 and 1000 nm is only about 0.2 eV, which is a typical level of accuracy for TD DFT calculations) and strong absorptions at 450 and 500 nm (Figure S9). Importantly, when the bridging group is chosen to be an *oxo* group in **4**, instead of hydroxo, the predicted TD DFT UV−vis spectrum is in quite *poor* agreement with experiment; in particular, no absorptions with significant oscillator strength are predicted beyond 670 nm, and only rather weak absorptions are predicted from 450 to 600 nm. When combined with the electrochemical predictions, these results provide strong support for the bridging ligand in **4** remaining as a hydroxo group.

In conclusion, available experimental and theoretical evidence supports formulations of the products of the 1- and 2-electron oxidation of **2** as the hydroxo-bridged localized mixed-valent Cu(III)Cu(II) and symmetric Cu(III)Cu(III) complexes **3** and **4**, respectively (recognizing that the electronic structure includes substantial Cu−O and Cu−N covalency). With the identification of these new species, a basis is provided for postulating such intermediates in oxidations promoted by copper sites in enzymes and other catalysts. Further examination of their structures and reactivity is warranted in view of their intriguing properties and potential involvement in catalysis.

■ ASSOCIATED CONTENT

Ⓢ Supporting Information

Synthetic details, spectroscopic and theoretical data, and crystallographic data (CIF). This material is available free of charge via the Internet at http://pubs.acs.org.

■ AUTHOR INFORMATION

Corresponding Authors
cramer@umn.edu
wtolman@umn.edu

■ REFERENCES

(1) Alvarez-Galvan, M. C.; Mota, N.; Ojeda, M.; Rojas, S.; Navarro, R. M.; Fierro, J. L. G. *Catal. Today* **2011**, *171*, 15−23.

(2) Schwarz, H. *Angew. Chem., Int. Ed.* **2011**, *50*, 10096−10115.

(3) Culpepper, M. A.; Rosenzweig, A. C. *Crit. Rev. Biochem. Mol. Biol.* **2012**, *47*, 483−492.

(4) Alayon, E. M. C.; Nachtegaal, M.; Ranocchiari, M.; van Bokhoven, J. A. *CHIMIA* **2012**, *66*, 668−674.

(5) Culpepper, M. A.; Cutsail, G. E., III; Hoffman, B. M.; Rosenzweig, A. C. *J. Am. Chem. Soc.* **2012**, *134*, 7640−7643. Balasubramanian, R.; Smith, S. M.; Rawat, S.; Yatsunyk, L. A.; Stemmler, T. L.; Rosenzweig, A. C. *Nature* **2010**, *465*, 115−119.

(6) Chan, S. I.; Yu, S. S. F. *Acc. Chem. Res.* **2008**, *41*, 969−979.

(7) Shiota, Y.; Yoshizawa, K. *Inorg. Chem.* **2009**, *48*, 838−845.

(8) Himes, R. A.; Karlin, K. D. *Curr. Opin. Chem. Biol.* **2009**, *13*, 119−131.

(9) Que, L., Jr.; Tolman, W. B. *Angew. Chem., Int. Ed.* **2002**, *41*, 1114−1137. Mirica, L. M.; Ottenwaelder, X.; Stack, T. D. P. *Chem. Rev.* **2004**, *104*, 1013−1045.

(10) Haack, P.; Kärgel, A.; Greco, C.; Dokic, J.; Braun, B.; Pfaff, F. F.; Mebs, S.; Ray, K.; Limberg, C. *J. Am. Chem. Soc.* **2013**, *135*, 16148−16160. Haack, P.; Limberg, C. *Angew. Chem., Int. Ed.* **2014**, *53*, 4282−4293.

(11) Woertink, J. S.; Smeets, P. J.; Groothaert, M. H.; Vance, M. A.; Sels, B. F.; Schoonheydt, R. A.; Solomon, E. I. *Proc. Natl. Acad. Sci. U.S.A.* **2009**, *106*, 18908−18913. Vanelderen, P.; Hadt, R. G.; Smeets, P. J.; Solomon, E. I.; Schoonheydt, R. A.; Sels, B. F. *J. Catal.* **2011**, *284*, 157−164.

(12) Donoghue, P. J.; Gupta, A. K.; Boyce, D. W.; Cramer, C. J.; Tolman, W. B. *J. Am. Chem. Soc.* **2010**, *132*, 15869−15871. Pirovano, P.; Magherusan, A. M.; McGlynn, C.; Ure, A.; Lynes, A.; McDonald, A. R. *Angew. Chem., Int. Ed.* **2014**, DOI: DOI: 10.1002/anie.201311152.

(13) Donoghue, P. J.; Tehranchi, J.; Cramer, C. J.; Sarangi, R.; Solomon, E. I.; Tolman, W. B. *J. Am. Chem. Soc.* **2011**, *133*, 17602−17605.

(14) Tehranchi, J.; Donoghue, P. J.; Cramer, C. J.; Tolman, W. B. *Eur. J. Inorg. Chem.* **2013**, *2013*, 4077−4084.

(15) Halvagar, M. R.; Tolman, W. B. *Inorg. Chem.* **2013**, *52*, 8306−8308.

(16) Mo, Z.; Yang, W.; Gao, J.; Chen, H.; Kang, J. *Synth. Commun.* **1999**, *29*, 2147−2153. Lin, J.; Lin, H.; Chen, J.-W.; Guo, Z. *Acta Crystallogr.* **2005**, *E61*, 1592−1594. Vandromme, L.; Monchaud, D.; Teulade-Fichou, M.-P. *Synlett* **2006**, 3423−3426.

(17) Butcher, R. J.; O'Connor, C. J.; Sinn, E. *Inorg. Chem.* **1981**, *20*, 537−545. El-Toukhy, A.; Cai, G. Z.; Davies, G.; Gilbert, T. R.; Onan, K. D.; Veidis, M. *J. Am. Chem. Soc.* **1984**, *106*, 4596−4605. McKee, V.; Tandon, S. S. *Inorg. Chem.* **1989**, *28*, 2901−2902. Agnus, Y.; Louis, R.; Metz, B.; Boudon, C.; Gisselbrecht, J. P.; Gross, M. *Inorg. Chem.* **1991**, *30*, 3155−3161. Atria, A. M.; Vega, A.; Contreras, M.; Valenzuela, J.; Spodine, E. *Inorg. Chem.* **1999**, *38*, 5681−5685. Bera, M.; Wong, W.

T.; Aromi, G.; Ribas, J.; Ray, D. *Inorg. Chem.* **2004**, *43*, 4787−4789. Voitekhovich, S. V.; Gaponik, P. N.; Lyakhov, A. S.; Filipova, J. V.; Sukhanova, A. G.; Sukhanov, G. T.; Ivashkevich, O. A. *Tetrahedron Lett.* **2009**, *50*, 2577−2579. Escuer, A.; Vlahopoulou, G.; Perlepes, S. P.; Mautner, F. A. *Inorg. Chem.* **2011**, *50*, 2468−2478. Löw, S.; Becker, J.; Würtele, C.; Miska, A.; Kleeberg, C.; Behrens, U.; Walter, O.; Schindler, S. *Chem.—Eur. J.* **2013**, *19*, 5342−5351.

(18) Perdew, J. P.; Burke, K.; Ernzerhof, M. *Phys. Rev. Lett.* **1996**, *77*, 3865−3868.

(19) Tomasi, J.; Mennucci, B.; Cances, E. *J. Mol. Struct. (Theochem)* **1999**, *464*, 211−226.

(20) Marenich, A. V.; Cramer, C. J.; Truhlar, D. G. *J. Phys. Chem. B* **2009**, *113*, 6378−6396.

(21) Peverati, R.; Truhlar, D. G. *J. Phys. Chem. Lett.* **2011**, *3*, 117−124.

(22) Marenich, A. V.; Majumdar, A.; Lenz, M.; Cramer, C. J.; Truhlar, D. G. *Angew. Chem., Int. Ed.* **2012**, *51*, 12810−12814.

(23) Marenich, A. V.; Cramer, C. J.; Truhlar, D. G.; Guido, C. A.; Mennucci, B.; Scalmani, G.; Frisch, M. J. *Chem. Sci.* **2011**, *2*, 2143−2161.